Shared Steering Control Using Safe Envelopes for Obstacle Avoidance and Vehicle Stability

Stephen M. Erlien, Susumu Fujita, and Joseph Christian Gerdes

***Abstract*—Steer-by-wire technology enables vehicle safety systems to share control with a driver through augmentation of the driver's steering commands. Advances in sensing technologies empower these systems further with real-time information about the surrounding environment. Leveraging these advancements in vehicle actuation and sensing, the authors present a shared control framework for obstacle avoidance and stability control using two safe driving envelopes. One of these envelopes is defined by the vehicle handling limits, whereas the other is defined by spatial limitations imposed by lane boundaries and obstacles. A model predictive control (MPC) scheme determines at each time step if the current driver command allows for a safe vehicle trajectory within these two envelopes, intervening only when such a trajectory does not exist. In this way, the controller shares control with the driver in a minimally invasive manner while avoiding obstacles and preventing loss of control. The optimal control problem underlying the controller is inherently nonconvex but is solved as a set of convex problems allowing for reliable real-time implementation. This approach is validated on an experimental vehicle working with human drivers to negotiate obstacles in a low friction environment.**

***Index Terms*—Vehicle dynamics, vehicle control, stability, envelope, predictive control, obstacle avoidance, shared control.**

I. Introduction

NEW technologies are empowering modern vehicles like never before. Sensing technologies like radar, cameras, and laser systems provide rich information about the environment in real time. Actuation technologies like steer-by-wire provide a means to augment a driver's steering command, giving automated systems significant control over the lateral dynamics of the vehicle. In addition, tire road friction estimates and vehicle states can be made available in real time in vehicles equipped with steer-by-wire, as demonstrated by Hsu *et al.* [1]. With these enhanced sensing and actuation capabilities, active safety systems have the potential to make cars much safer.

However, the best way to utilize these advancements to improve passenger safety remains an open-ended question. Fully automated driving is a tempting solution, but it requires automating the many social and cognitive aspects of driving. Shared control schemes in which a human driver and an automated system work together present an opportunity to leverage these sensing and actuation capabilities while still retaining the abilities of human drivers. In addition, shared control enables drivers who enjoy driving to continue to do so with improved safety. With respect to obstacle avoidance and lane keeping, a number of approaches to shared control have been proposed.

One approach is to only guide the driver without actively controlling the vehicle. This leaves the human driver always in full control. Kawabe *et al.* present such an approach using a Model Predictive Control (MPC) framework that leverages information about the surrounding environment to generate optimal paths to help guide a human driver [2].

Another approach is to explicitly switch control between a human driver and an automated controller. Minoiu-Enache *et al.* present a lane departure avoidance system for steer-by-wire vehicles which switches control between a human and a number of control laws depending on the measured attentiveness of the driver [3]. Gray *et al.* use a hierarchical MPC approach for path planning and path tracking that switches control to and from the driver as a function of driver attentiveness [4].

In contrast to switching control, another shared control approach involves the interpretation of the driver's intention and a controller that seeks to track this interpreted intent. Gao *et al.* present MPC approaches with a given trajectory representing the driver's intent [5]. Saleh *et al.* present a lane keeping driver assistance system formulated as a preview horizon optimal control problem using a driver-vehicle-road model to predict the driver's behavior [6].

Another approach to shared control, which is most similar to the approach proposed in this paper, uses a final steer command which is a blend of a human driver and an optimal controller. Anderson *et al.* use such a constraint-based, pathless MPC approach to share control of teleoperated ground vehicles so that the controller's influence on the final command increases with the severity of the predicted maneuver [7].

Instead of blending the driver's and controller's commands, the method proposed in this paper incorporates the driver's steer command directly into the problem formulation. In this way, matching the driver's present steer command becomes a control objective that is evaluated against the additional objectives of collision avoidance and vehicle stability. In considering only the driver's present steering command, no model or interpretation of the driver's intentions is required. In addition, no logic or heuristics are necessary to determine when to switch control between human and controller; the controller is always in control

Manuscript received March 11, 2014; revised August 4, 2014, November 17, 2014, and April 15, 2015; accepted June 4, 2015. Date of publication November 4, 2015; date of current version January 29, 2016. The Associate Editor for this paper was L. Vlacic.

S. M. Erlien was with the Dynamic Design Laboratory, Department of Mechanical Engineering, Stanford University, Stanford, CA 94305 USA. He is now with Peloton Technology, Mountain View, CA 94043 USA (e-mail: serlien@alumni.stanford.edu).

S. Fujita is with Nissan Motor Company Ltd., Atsugi 243-0123, Japan.

J. C. Gerdes is with the Dynamic Design Laboratory, Department of Mechanical Engineering, Stanford University, Stanford, CA 94305 USA.

Color versions of one or more of the figures in this paper are available online at http://ieeexplore.ieee.org.

Digital Object Identifier 10.1109/TITS.2015.2453404

but is biased to identically match the driver's command whenever it is safe to do so. In this way, the proposed controller implements a form of envelope control, which is characterized by safe regions, or envelopes, of the state space in which a human operator is free to operate with the controller intervening only to ensure operation remains within these safe regions. Envelope control is widely used in aircraft control, as described by Well [8], and has recently been applied to vehicle stability by Beal and Gerdes using an MPC framework [9].

In addition to ensuring vehicle stability, the presented controller incorporates a collision avoidance objective. A number of approaches to generating collision-free trajectories using safe envelopes have been proposed in the context of autonomous vehicle navigation. Attia *et al.* identify a safe region, or validity area, for the generation of a collision-free trajectory which is then tracked by a nonlinear MPC based controller [10]. Hundelshausen *et al.* use precalculated trajectories to fan out tentacle like structures to identify safe regions for vehicle navigation [11]. The approach proposed in this paper also identifies open space for use in planning collision-free trajectories.

The predictive nature and constraint handling capabilities of MPC make it an attractive framework for implementing this approach to shared control which considers the trade-off between vehicle stability and obstacle avoidance. MPC was also used by Carlson and Gerdes in the real-time consideration of vehicle stability and rollover prevention [12]. The MPC implementation used in this work builds upon prior work by the authors [13] and makes use of variable length time steps in the prediction horizon to enable look ahead times long enough for obstacle avoidance while still capturing the fast dynamics of the vehicle in the near-term. This results in a control scheme that is simple enough for fast, real-time consideration of vehicle stability and obstacle avoidance. In addition, the choice of penalty functions and relative weights on the envelope slack variables influences the trade-off between vehicle stability and obstacle avoidance that the controller is capable of making in real time. This is illustrated in experimentation on a vehicle testbed working with human drivers to navigate limited friction environments.

The remainder of this paper is structured as follows. Section II outlines the vehicle model used by the real-time controller. Section III derives the safe driving envelopes and describes the methodologies for generating these envelopes in real time. Section IV presents the MPC formulation along with the underlying convex optimization problem(s) to be solved at each time step. Lastly, experimental results demonstrate smooth integration of the driver's and controller's commands as well as the combined stabilizing and obstacle avoidance capabilities of the control framework.

II. Vehicle Model

The vehicle model used in the MPC controller is a bicycle model with five states: two velocity states and three position states. Table I gives the notation used to describe the vehicle model. In this paper, front steering is the only actuator considered, and the vehicle is assumed to be equipped with steer-by-wire technology which enables the steer angle of the front road wheels (δ) to differ from the driver's commanded front steer angle (δ_{driver}) which is inputted to the hand wheel. Also, the controller shares control with the driver in steering only, leaving the driver in full control of the vehicle's longitudinal dynamics. Without a direct influence on the vehicle's speed, the controller simply reacts to changes in speed dictated by the driver and, for simplicity, assumes the present vehicle speed will be maintained throughout the prediction horizon. Therefore, the vehicle model used by the controller assumes a constant longitudinal speed.

TABLE I
Vehicle Model Notation

Description	Symbol	Units
Steer angle	δ	rad
Longitudinal Speed	U_{x}	m/s
Lateral Speed	U_{y}	m/s
Sideslip	β	rad
Yaw rate	r	rad/s
Heading deviation from path	$\Delta\psi$	rad
Lateral deviation from path	e	m
Distance along the path	s	m
Lateral tire force on [front,rear] axle	$F_{\mathrm{y[f,r]}}$	N
Tire slip angle on [front,rear] axle	$\alpha_{\mathrm{[f,r]}}$	rad

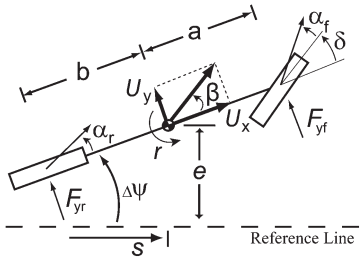

Fig. 1. Bike model schematic.

A. Velocity States

The velocity states are sideslip (β) and yaw rate (r) as defined in Fig. 1. The vehicle's sideslip can be expressed as:

$$\beta = \arctan\left(\frac{U_{\mathrm{y}}}{U_{\mathrm{x}}}\right) \tag{1}$$

$$\approx \frac{U_{\mathrm{y}}}{U_{\mathrm{x}}} \tag{2}$$

where U_{y} and U_{x} are the lateral and longitudinal velocities in the body fixed frame, respectively, and the assumption that $U_{\mathrm{x}} \gg U_{\mathrm{y}}$ gives the simplified expression.

Assuming U_{x} is constant, the vehicle's velocity states have the following equations of motion:

$$\dot{\beta} = \frac{F_{\mathrm{yf}} + F_{\mathrm{yr}}}{mU_{\mathrm{x}}} - r \tag{3}$$

$$\dot{r} = \frac{aF_{\mathrm{yf}} - bF_{\mathrm{yr}}}{I_{\mathrm{zz}}} \tag{4}$$

where $F_{\mathrm{y[f,r]}}$ is the lateral tire force of the [front, rear] axle, m is the vehicle mass, I_{zz} is the yaw inertia, and a and b are the distances from the center of gravity to the front and rear axles, respectively.

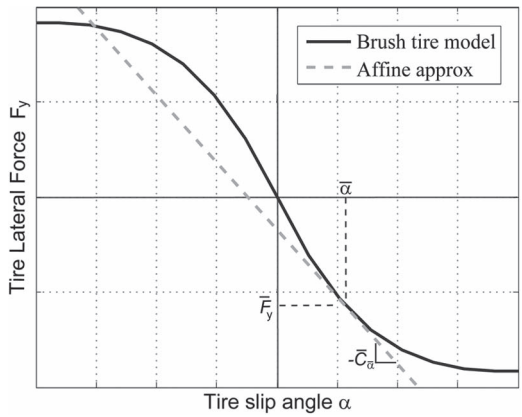

Fig. 2. Brush tire model with affine approximation at $\bar{\alpha}$.

The tire slip angle in the front (α_{f}) and rear (α_{r}) can be expressed as:

$$\begin{aligned}\alpha_{\mathrm{f}} &= \arctan\left(\beta + \frac{ar}{U_{\mathrm{x}}}\right) - \delta \\ &\approx \beta + \frac{ar}{U_{\mathrm{x}}} - \delta \end{aligned} \tag{5}$$

$$\begin{aligned}\alpha_{\mathrm{r}} &= \arctan\left(\beta - \frac{br}{U_{\mathrm{x}}}\right) \\ &\approx \beta - \frac{br}{U_{\mathrm{x}}} \end{aligned} \tag{6}$$

where small angle approximations give linear expressions. This approximation is validated by the stability constraints used by the controller as discussed in Section III-A.

The brush tire model proposed by Fiala [14] and presented in the following form by Pacejka [15] gives a useful model of the relationship between $F_{\mathrm{y[f,r]}}$ and $\alpha_{\mathrm{[f,r]}}$:

$$\begin{aligned} F_{\mathrm{y}} &= \begin{cases} -C_\alpha \tan\alpha + \frac{C_\alpha^2}{3\mu F_{\mathrm{z}}} |\tan\alpha| \tan\alpha \\ \quad -\frac{C_\alpha^3}{27\mu^2 F_{\mathrm{z}}^2} \tan^3\alpha, & |\alpha| < \arctan\left(\frac{3\mu F_{\mathrm{z}}}{C_\alpha}\right) \\ -\mu F_{\mathrm{z}} \mathrm{sgn}\,\alpha, & \text{otherwise} \end{cases} \\ &= f_{\mathrm{tire}}(\alpha) \end{aligned} \tag{7}$$

where μ is the surface coefficient of friction, $F_{\mathrm{z[f,r]}}$ is the normal load, and $C_{\alpha\mathrm{[f,r]}}$ is the tire cornering stiffness. This tire force model is illustrated in Fig. 2. The vehicle's tire cornering stiffness, $C_{\alpha\mathrm{[f,r]}}$, is determined from experimental data from steady-state maneuvers.

The nonlinearity of the tire forces poses a significant challenge to real-time optimization. To address this challenge, the vehicle model used by the MPC controller describes the vehicle's behavior by using tire forces and not steer angles. Front tire force (F_{yf}) serves as the input to the model and is mapped to δ using (5) and (7):

$$\delta = \beta + \frac{ar}{U_{\mathrm{x}}} - f_{\mathrm{tire}}^{-1}(F_{\mathrm{yf}}) \tag{8}$$

where real-time estimates of β and r are assumed to be available and f_{tire}^{-1} is computed numerically and implemented as a 2D lookup table with inputs of rear slip angle and surface friction estimate. Use of F_{yf} as the model input allows for a linear vehicle model which considers front tire saturation.

For the rear tires, a linearization of the brush tire model at a given rear tire slip angle $(\bar{\alpha}_{\mathrm{r}})$ models rear tire force (F_{yr}) as an affine function of α_{r}:

$$F_{\mathrm{yr}} = \bar{F}_{\mathrm{yr}} - \bar{C}_{\bar{\alpha}_{\mathrm{r}}}(\alpha_{\mathrm{r}} - \bar{\alpha}_{\mathrm{r}}) \tag{9}$$

where $\bar{F}_{\mathrm{yr}} = f_{\mathrm{tire}}(\bar{\alpha}_{\mathrm{r}})$ and $\bar{C}_{\bar{\alpha}_{\mathrm{r}}}$ is the equivalent cornering stiffness at $\bar{\alpha}_{\mathrm{r}}$. This approximation is also illustrated in Fig. 2. Choosing the current rear slip angle, α_{r}, to be $\bar{\alpha}_{\mathrm{r}}$ in the initial time steps of the prediction horizon allows the MPC controller to explicitly consider rear tire saturation in the near-term prediction [9]. This will be discussed further in Section IV. For simplicity, tire model (7) is only a function of slip angle; however, force coupling due to the driver controlled longitudinal force could be directly included in the tire model as demonstrated in a real-time MPC scheme by Beal and Gerdes [9].

The equations of motion of the velocity states can now be expressed as affine functions of the states and input, F_{yf}:

$$\dot{\beta} = \frac{F_{\mathrm{yf}} + \bar{F}_{\mathrm{yr}} - \bar{C}_{\bar{\alpha}_{\mathrm{r}}}\left(\beta - \frac{br}{U_{\mathrm{x}}} - \bar{\alpha}_{\mathrm{r}}\right)}{mU_{\mathrm{x}}} - r \tag{10}$$

$$\dot{r} = \frac{aF_{\mathrm{yf}} - b\left[\bar{F}_{\mathrm{yr}} - \bar{C}_{\bar{\alpha}_{\mathrm{r}}}\left(\beta - \frac{br}{U_{\mathrm{x}}} - \bar{\alpha}_{\mathrm{r}}\right)\right]}{I_{\mathrm{zz}}}. \tag{11}$$

B. Position States

The position states of the vehicle are all in reference to a reference line that is assumed to be known but need not be obstacle-free. These states are heading deviation $(\Delta\psi)$, lateral deviation (e), and distance along the path (s) as defined in Fig. 1.

The equations of motion of the position states can be written as:

$$\dot{\Delta\psi} = r \tag{12}$$

$$\dot{e} = U_{\mathrm{x}} \sin(\Delta\psi) + U_{\mathrm{y}} \cos(\Delta\psi) \tag{13}$$

$$\dot{s} = U_{\mathrm{x}} \cos(\Delta\psi) - U_{\mathrm{y}} \sin(\Delta\psi) \tag{14}$$

Using small angle assumptions for $\Delta\psi$ and β, the above nonlinear equations can be approximated as linear functions of the vehicle states:

$$\dot{e} \approx U_{\mathrm{x}}\Delta\psi + U_{\mathrm{x}}\beta \tag{15}$$

$$\begin{aligned}\dot{s} &\approx U_{\mathrm{x}} - U_{\mathrm{x}}\beta\Delta\psi \\ &\approx U_{\mathrm{x}} \end{aligned} \tag{16}$$

where, for small values of β and $\Delta\psi$, the product $\beta\Delta\psi \approx 0$. The small angle assumption for β is a weaker assumption because, as described in Section III-A, the controller bounds sideslip explicitly. The small angle assumption for $\Delta\psi$ is a stronger assumption because the controller does not directly bound this state; however, to avoid collision with the road

boundaries, the controller indirectly maintains $\Delta\psi$ around zero as demonstrated in the experimental results.

Combining (10), (11), (12), (15) and (16), a continuous state-space representation of the vehicle model can be expressed as:

$$\dot{x} = A_{\mathrm{c}}(\bar{\alpha}_{\mathrm{r}})x + B_{\mathrm{c}}F_{\mathrm{yf}} + d_{\mathrm{c}}(\bar{\alpha}_{\mathrm{r}}) \tag{17}$$

With

$$x = \begin{bmatrix}\beta & r & \Delta\psi & s & e\end{bmatrix}^T$$

$$A_{\mathrm{c}}(\bar{\alpha}_r) = \begin{bmatrix} -\frac{\bar{C}_{\bar{\alpha}_{\mathrm{r}}}}{mU_{\mathrm{x}}} & \frac{b\bar{C}_{\bar{\alpha}_{\mathrm{r}}}}{mU_{\mathrm{x}}^2} - 1 & 0 & 0 & 0 \\ \frac{b\bar{C}_{\bar{\alpha}_{\mathrm{r}}}}{I_{zz}} & -\frac{b^2\bar{C}_{\bar{\alpha}_{\mathrm{r}}}}{I_{zz}U_{\mathrm{x}}} & 0 & 0 & 0 \\ 0 & 1 & 0 & 0 & 0 \\ 0 & 0 & 0 & 0 & 0 \\ U_{\mathrm{x}} & 0 & U_{\mathrm{x}} & 0 & 0 \end{bmatrix}$$

$$B_{\mathrm{c}} = \begin{bmatrix}\frac{1}{mU_{\mathrm{x}}} & \frac{a}{I_{zz}} & 0 & 0 & 0\end{bmatrix}^T$$

$$d_{\mathrm{c}}(\bar{\alpha}_{\mathrm{r}}) = \begin{bmatrix}\frac{\bar{F}_{\mathrm{yr}}+\bar{\alpha}_{\mathrm{r}}\bar{C}_{\bar{\alpha}_{\mathrm{r}}}}{mU_{\mathrm{x}}} & -\frac{b(\bar{F}_{\mathrm{yr}}+\bar{\alpha}_{\mathrm{r}}\bar{C}_{\bar{\alpha}_{\mathrm{r}}})}{I_{zz}} & 0 & U_{\mathrm{x}} & 0\end{bmatrix}^T$$

where subscript c denotes a continuous time model and $(\bar{\alpha}_{\mathrm{r}})$ indicates linearization around $\bar{\alpha}_{\mathrm{r}}$.

III. Envelope Definitions

To ensure safe operation of the vehicle, the controller confines the states of the vehicle to remain within two safe driving envelopes over a finite prediction horizon. The first of these is a stable handling envelope that ensures vehicle stability through constraints on the velocity states. The second is an environmental envelope that constrains the position states to ensure the vehicle trajectory is collision-free. The definitions of these envelopes and the methodologies to generate them in real time are presented in the following sections.

A. Stable Handling Envelope

The stable handling envelope used in this paper was originally presented by Beal and Gerdes [9]. However, other vehicle stability envelopes have been proposed [16] and could be incorporated into this framework as well.

The stable handling envelope defines limits on the vehicle's velocity states as illustrated in Fig. 3. This envelope is bounded by the steady-state yaw rate and the rear slip angle at peak tire force. These bounds reflect the maximum capabilities of the vehicle's tires, and at any point within this envelope, there exists a steering command that directs the vehicle to safely remain inside. Outside of this envelope, there is no guarantee that the vehicle can move monotonically towards the boundary. However, leaving this boundary does not mean the vehicle will go unstable. Should the vehicle be perturbed outside of this boundary, either by controller action to avoid collision or by a change in road conditions, there is a large region of the state space in which the controlled vehicle will return safely to the stable handling envelope.

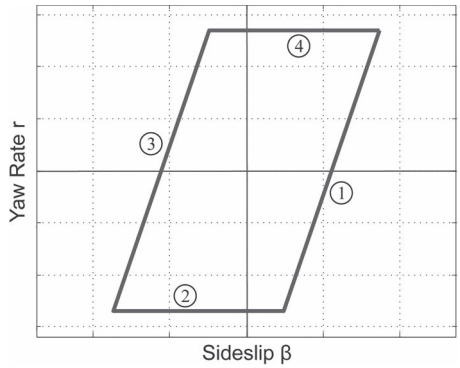

Fig. 3. Stable handling envelope.

A steady-state analysis can be used to determine an appropriate bound on yaw rate that does not exceed the friction capabilities of the vehicle. Considering the steady-state condition of (3), the steady-state yaw rate can be expressed as:

$$r_{\mathrm{ss}} = \frac{F_{\mathrm{yf}} + F_{\mathrm{yr}}}{mU_{\mathrm{x}}}. \tag{18}$$

Neglecting the effects of weight transfer and assuming zero longitudinal tire forces, the following relationship holds:

$$F_{\mathrm{yf,max}} + F_{\mathrm{yr,max}} = mg\mu \tag{19}$$

where g is the gravitational constant.

Combining (18) and (19) gives an expression for the maximum steady-state yaw rate which defines bounds ② and ④ in Fig. 3:

$$r_{\mathrm{ss,max}} = \frac{g\mu}{U_{\mathrm{x}}}. \tag{20}$$

Another important consideration for vehicle stability is the saturation of the rear tires. The final two bounds of the vehicle envelope serve to limit the rear slip angle to the angle at which lateral force saturates $(\alpha_{\mathrm{r,sat}})$. For brush tire model (7), this is expressed as:

$$\alpha_{\mathrm{r,sat}} = \arctan\left(3\frac{mg\mu}{C_{\alpha_{\mathrm{r}}}}\frac{a}{a+b}\right). \tag{21}$$

Using the vehicle parameters and surface friction estimate from the experiments described in Section V, $\alpha_{\mathrm{r,sat}} = 7.2$ (deg), giving validation to the small angle approximations made in (5) and (6). Using this expression as a bound on α_{r}, the following bound on β can be determined from (6):

$$\beta_{\max} = \alpha_{\mathrm{r,sat}} + \frac{br}{U_{\mathrm{x}}}. \tag{22}$$

This maximum sideslip serves as the basis for bounds ① and ③ in Fig. 3. Assuming real-time estimates of μ, r, and U_{x} are available, the vehicle envelope described is easily calculated in

real time and can be compactly represented as the following linear inequality for each time step k into the prediction horizon:

$$H_{\mathrm{sh}} x^{(k)} \leq G_{\mathrm{sh}} \tag{23}$$

with

$$H_{\mathrm{sh}} = \begin{bmatrix} 1 & -\frac{b}{U_{\mathrm{x}}} & 0 & 0 & 0 \\ 0 & 1 & 0 & 0 & 0 \\ -1 & \frac{b}{U_{\mathrm{x}}} & 0 & 0 & 0 \\ 0 & -1 & 0 & 0 & 0 \end{bmatrix}$$

$$G_{\mathrm{sh}} = \begin{bmatrix} \alpha_{\mathrm{r,sat}} \\ r_{\mathrm{ss,max}} \\ \alpha_{\mathrm{r,sat}} \\ r_{\mathrm{ss,max}} \end{bmatrix}$$

where subscript sh denotes the stable handling envelope and $x^{(k)}$ indicates the vehicle state at the kth time step into the prediction horizon.

B. Environmental Envelope

The environmental envelope is in reference to the same reference line as the position states of the vehicle model. It is represented as time-varying constraints on e, the lateral deviation from the reference line. At each time step, the trajectory of the vehicle over the prediction horizon is constrained to be within this envelope to ensure the trajectory is collision-free. As mentioned previously, this reference line need not be obstacle-free; therefore, the environmental envelope may require the vehicle to deviate from the reference line.

Fig. 4 illustrates the methodology to generate the environmental envelope from a collection of obstacles along the reference line as illustrated in Fig. 4(a). As stated previously, the controller shares control with the driver in steering, leaving the driver in full control of the longitudinal dynamics of the vehicle. Without a direct influence on the vehicle's speed, the controller simply reacts to changes in speed dictated by the driver and for simplicity assumes the present vehicle speed will be maintained throughout the prediction horizon. This allows for the environment to be sampled at discrete points along the reference line, which correspond to the vehicle's future position k steps into the prediction horizon as illustrated in Fig. 4(b). In Fig. 4(c), the objects in the environment are extended to align with this discrete sampling, and feasible gaps between obstacles are identified producing a representation of the obstacle-free regions of the environment. Feasible gaps are defined as distances greater than the vehicle width. Each feasible gap can be thought of as a cell in a variant of the vertical cell decomposition described by LaValle [17].

Starting at the vehicle's current position and moving in the positive s direction, adjacent feasible gaps are linked using a graph search algorithm to form tubes through the environment like the two illustrated in Fig. 4(d). To avoid collision with the environment, the vehicle's future trajectory needs to be fully contained within one of these tubes. This concept of feasible

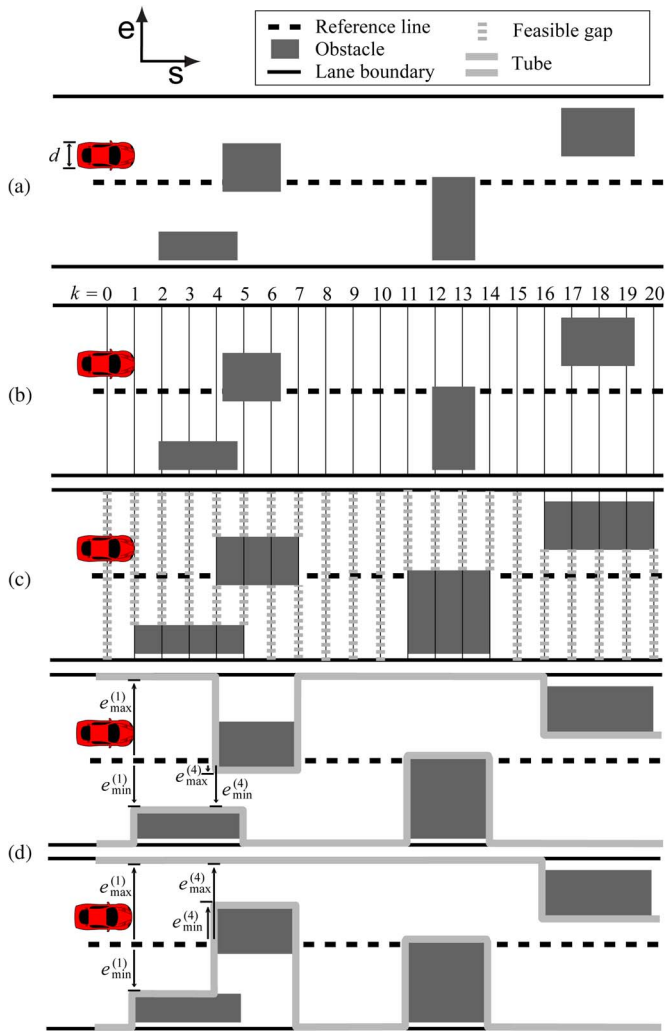

Fig. 4. Generating the environmental envelope. Start with a) a collection of obstacles along the reference line, b) discretize in the s direction, c) extend objects in s direction to align with discretization and identify feasible gaps between objects, and then d) connect adjacent gaps into tubes (two of them in this example) which each define a maximum $(e_{\mathrm{max}}^{(k)})$ and minimum $(e_{\mathrm{min}}^{(k)})$ lateral deviation from the reference line at each time step, k.

tubes has also been used in motion planning for robotic arms as presented by Suh and Bishop [18].

Each tube defines a bound on e at each time step k to ensure collision avoidance and can be compactly written as the linear inequality:

$$H_{\mathrm{env}} x^{(k)} \leq G_{\mathrm{env}}^{(k)} \tag{24}$$

with

$$H_{\mathrm{env}} = \begin{bmatrix} 0 & 0 & 0 & 0 & 1 \\ 0 & 0 & 0 & 0 & -1 \end{bmatrix}$$

$$G_{\mathrm{env}} = \begin{bmatrix} e_{\mathrm{max}}^{(k)} - \frac{1}{2}d - d_{\mathrm{buffer}} \\ -e_{\mathrm{min}}^{(k)} - \frac{1}{2}d - d_{\mathrm{buffer}} \end{bmatrix}$$

where the subscript env denotes the environmental envelope, $e_{\mathrm{max}}^{(k)}$ and $e_{\mathrm{min}}^{(k)}$ indicate the lateral deviation bounds for time

step k, d is the vehicle width, and d_{buffer} specifies an added distance between obstacles and the vehicle's sides to ensure driver comfort. The distance of d_{buffer} also accounts for the additional minimum gap between obstacles required as the vehicle's orientation changes. The environmental envelope is defined as the set of tubes generated as described above, and a vehicle trajectory is collision-free throughout the prediction horizon if and only if it satisfies inequality (24) for all k for any *one* tube in the environmental envelope.

IV. MPC Formulation

The controller's primary task is to ensure safe vehicle operation within the previously defined safe driving envelopes. With these objectives met, it is desirable to be minimally invasive to the driver while avoiding harsh interventions by the controller. The first of these objectives is modeled in this work as identically matching the driver's present steering command, and the latter is modeled as a preference for future trajectories with smooth steering commands. These objectives can be expressed as an optimal control problem to be evaluated over a finite prediction horizon. However, the set of feasible, collision-free trajectories to be evaluated is a non-convex set due to the presence of obstacles making the underlying control problem difficult to solve directly.

Instead, a simpler, convex sub-problem is solved for each tube in the environmental envelope, and the solutions to these sub-problems are compared to give the global optimum to the non-convex control problem underlying the MPC controller. This is possible because any convex combination of trajectories that are generated from vehicle model (7) and are contained within a tube will also be contained within that same tube. Therefore, each tube defines a convex set of collision-free trajectories which enables the use of fast convex optimization techniques to quickly identify an optimal trajectory within a given tube. Dividing the environment into possible tubes transforms a non-convex problem into a set of convex problems which can be quickly solved. These sub-problems could be solved in parallel to further improve performance.

A. Two Time Scale Prediction Horizon

The obstacle avoidance objective of the controller necessitates a long enough prediction horizon to safely anticipate upcoming obstacles; however, if the controller execution time step, $t_{\text{s,MPC}}$, is used as the prediction time step throughout the full horizon, the total number of time steps required is prohibitively large for real-time implementation. Alternatively, selecting a large time step for the full horizon degrades the controller's performance in predicting near-term vehicle behavior which is necessary when reacting to unexpected challenges to vehicle stability. In addition, it is important to capture the limited slew capabilities of the steering system in the near-term when attempting to match the driver's steering command while adhering to the safe handling envelope.

To address this issue, the prediction horizon used in this work is split into two portions. The initial portion is comprised of T_{split} small time steps of size $t_{\text{s,MPC}} = 0.01$ (s) to accurately capture near-term vehicle behavior and steering system slew rate limitations. The latter portion is comprised of larger time steps of size $t_{\text{s,long}} = 0.2$ (s) to extend the horizon to incorporate upcoming obstacles in the long-term. There are T steps in the complete prediction horizon, which is largely dictated by computational limitations. These time step sizes provide a good balance between look ahead distance and environment resolution and are comparable to those used in other MPC implementations for vehicle control [5].

B. Convex Optimization Problem(s)

At each execution of the controller, optimization problem (25) is solved for each tube in the environmental envelope, and the optimal input corresponding to the tube with the lowest objective value is used. As is common with MPC, only the optimal input for the first step into the prediction horizon, $F^{(0)}_{\text{yf,opt}}$, is applied to the vehicle, and the optimization problem is re-solved for all tubes at the next time step without any regard for which tube generated the optimal input previously. Therefore, the driver is never restricted to a specific tube, but is free to switch to whichever tube best meets the control objectives. In this way, the tube construct is used only to facilitate computation of the global solution to the non-convex optimal control problem underlying the controller, and, therefore, has no effect on the stability properties of the MPC controller.

The control objectives outlined previously can be expressed as the following receding horizon optimal control problem:

$$\begin{aligned}
\text{minimize} \quad & \left| F_{\text{yf,driver}} - F^{(0)}_{\text{yf,opt}} \right| && \text{(25a)}\\
& + \sum_{k=0}^{(T-1)} \gamma^{(k)} \left(F^{(k)}_{\text{yf,opt}} - F^{(k-1)}_{\text{yf,opt}} \right)^2 && \text{(25b)}\\
& + \sum_{k=0}^{(T-1)} \begin{bmatrix} \sigma_{\text{sh}} & \sigma_{\text{sh}} \end{bmatrix} \left| S^{(k+1)}_{\text{sh,opt}} \right| && \text{(25c)}\\
& + \sum_{l=(T_{\text{split}}+1)}^{T} \begin{bmatrix} \sigma_{\text{env}} & \sigma_{\text{env}} \end{bmatrix} \left(S^{(l)}_{\text{env,opt}} \right)^2 && \text{(25c)}\\
\text{subject to} \quad & x^{(k+1)} = A^{(k)}_d x^{(k)} + B^{(k)}_d F^{(k)}_{\text{yf,opt}} + d^{(k)}_d && \text{(25e)}\\
& \left| F^{(k)}_{\text{yf,opt}} \right| \leq F_{\text{yf,max}} && \text{(25f)}\\
& H_{\text{sh}} x^{(k+1)} \leq G_{\text{sh}} + S^{(k+1)}_{\text{sh,opt}} \\
& \qquad k = 0 \ldots (T-1) && \text{(25g)}\\
& H_{\text{env}} x^{(l)} \leq G^{(l)}_{\text{env}} + S^{(l)}_{\text{env,opt}} \\
& \qquad l = (T_{\text{split}}+1) \ldots T && \text{(25h)}\\
& \left| F^{(i)}_{\text{yf,opt}} - F^{(i-1)}_{\text{yf,opt}} \right| \leq F_{\text{yf,max slew}} \\
& \qquad i = 0 \ldots T_{\text{split}} && \text{(25i)}
\end{aligned}$$

where $\sigma_{\text{sh}} \in \mathbb{R}^{(1,2)}$, $\sigma_{\text{env}} \in \mathbb{R}$, and $\bullet^2$ indicates an element-wise square operation. In this optimization problem, the variables

to be optimized are the input trajectory ($F_{\mathrm{yf,opt}}$) and the safe driving envelope slack variables ($S_{\mathrm{sh,opt}}, S_{\mathrm{env,opt}}$). The optimal force command applied to the vehicle on the previous time step is represented as $F_{\mathrm{yf,opt}}^{(-1)}$ and serves to ensure steering smoothness and slew constraints with respect to the previous steering command.

Tunable parameters in this optimization problem are γ, which establishes the trade-off between a smooth input trajectory (25b) and matching the driver's present steering command (25a), and the slack variable costs ($\sigma_{\mathrm{sh}}, \sigma_{\mathrm{env}}$). As a result of the two time scale prediction horizon, different values of γ are used in each portion of the horizon to give a more uniformly smooth trajectory over the entire horizon, as given by:

$$\gamma^{(k)} = \begin{cases} \gamma_{\mathrm{near}} & 0 \le k < T_{\mathrm{split}} \\ \gamma_{\mathrm{long}} & \text{otherwise} \end{cases} \tag{26}$$

where γ_{near} and γ_{long} correspond to the near and long-term portions of the horizon, respectively, and $\gamma_{\mathrm{near}} > \gamma_{\mathrm{long}}$.

Cost term (25a) expresses the desire to match the driver's command where $F_{\mathrm{yf,driver}}$ is the front tire force corresponding to the driver's commanded front steer angle, δ_{driver}. Brush tire model (7) provides the mapping from δ_{driver} to $F_{\mathrm{yf,driver}}$:

$$F_{\mathrm{yf,driver}} = f_{\mathrm{tire}}\left(\beta + \frac{ar}{U_x} - \delta_{\mathrm{driver}}\right). \tag{27}$$

Constraints (25g) and (25h) enforce the stable handling and environmental envelopes, respectively. Instead of enforcing these envelopes as hard constraints, slack variables, $S_{\mathrm{sh,opt}}$ and $S_{\mathrm{env,opt}}$, penalize violations of the envelopes, ensuring optimization problem (25) always has a feasible solution. With the choice of sufficiently large σ_{sh} and σ_{env}, cost terms (25c) and (25d) encourage zero-valued slack variables resulting in optimal vehicle trajectories which adhere to both safe driving envelopes whenever possible. A quadratic penalty function for the environmental envelope allows for smoother interactions at the envelope boundary and, along with the relative size of σ_{sh} and σ_{env}, establishes a hierarchy between the two safe driving envelopes. Choosing $\sigma_{\mathrm{env}} \gg \sigma_{\mathrm{sh}}$ enforces a preference for obstacle avoidance over vehicle stability in situations where the controller is forced to choose between adherence to one envelope in favor of the other as illustrated in the experimental results. With the weights chosen such that $\sigma_{\mathrm{env}} \gg \sigma_{\mathrm{sh}} \gg \gamma$, the behavior of the controller is not sensitive to the exact values of σ_{env} or σ_{sh}.

To ease the computation of optimization problem (25) and simplify the generation of the environmental envelope, constraint (25h) is not enforced in the early portion of the prediction horizon because steering has little influence on the position states of the vehicle over such a short time duration. Instead, the predictive nature of the MPC controller steers the vehicle in anticipation of approaching obstacles, guiding the vehicle to be collision-free over the short initial time steps without directly enforcing the environmental envelope in the near-term.

Constraint (25f) reflects the maximum force capabilities of the front tires and (25i) reflects the slew rate capabilities of the vehicle steering system. The slew rate constraint is not enforced during the later portion of the prediction horizon because the larger time steps make such a constraint ill-defined.

The vehicle models used in constraint (25e) are zero order hold discretizations of the continuous vehicle model (17) with $\bar{\alpha}_{\mathrm{r}}$ is given for the kth time step by:

$$\bar{\alpha}_{\mathrm{r}} = \begin{cases} \alpha_{\mathrm{r}}^{(0)} & 0 \le k < T_{\mathrm{split}} \\ 0 & T_{\mathrm{split}} \le k \le (T-1) \end{cases}$$

where $\alpha_r^{(0)}$ is the current rear slip angle determined by (6) from real-time estimates of β and r. In this way, the vehicle model used in the near-term prediction horizon is a linearization of the nonlinear rear tire behavior at the current rear slip angle ($\alpha_r^{(0)}$) allowing for consideration of rear tire saturation in the near-term horizon. As a consequence of this changing rear tire model, the discrete vehicle model is calculated on-line by the controller and used in the initial portion of the prediction horizon. In the remainder of the prediction horizon, the rear tire slip angle is not known prior to solving optimization (25); therefore, a linear rear tire model is used. The implications of this simplifying assumption are highlighted in the experimental results.

C. Varying Time Steps in Prediction Horizon

To enable consideration of approaching obstacles in the long-term without compromising the prediction of velocity states in the near-term, different length time steps are employed in the prediction horizon of the MPC formulation as described in Section IV-A. This results in the controller executing faster than the time step used in the long-term prediction horizon, and requires a corrective, variable length time step to ensure a consistent representation of the environment as illustrated in Fig. 5. Following the methodology for generating the environmental envelope described in Section III-B, the boundaries of an obstacle are extended to align with the discretization of the environment. Fig. 5(a) shows the discretization of the same environment a short time later without an initial correction time step resulting in a different representation of the obstacle; however, if a correction time step of appropriate length is used initially, the obstacle representation does not change as illustrated in Fig. 5(b).

This required correction time step length, $t_{\mathrm{s,corr}}$, can be defined recursively. At the first execution of the controller, $t_{\mathrm{s,corr}} = t_{\mathrm{s,MPC}}$, and thereafter is given by:

$$t_{\mathrm{s,corr}} = \begin{cases} t_{\mathrm{s,corr}}^{-} - \frac{\Delta s}{U_{\mathrm{x}}} & \left(t_{\mathrm{s,corr}}^{-} - \frac{\Delta s}{U_{\mathrm{x}}}\right) > t_{\mathrm{s,MPC}} \\ t_{\mathrm{s,corr}}^{-} - \frac{\Delta s}{U_{\mathrm{x}}} + t_{\mathrm{s,long}} & \text{otherwise} \end{cases} \tag{28}$$

where $t_{\mathrm{s,corr}}^{-}$ is the correction time step length on the previous execution of the controller and $\Delta s = s - s^{-}$ is the change in the vehicle's distance along the reference line since the previous execution of the controller. Using this correction time step in between the short and long time step portions of the prediction horizon ensures a consistent representation of the environment across multiple executions of the controller.

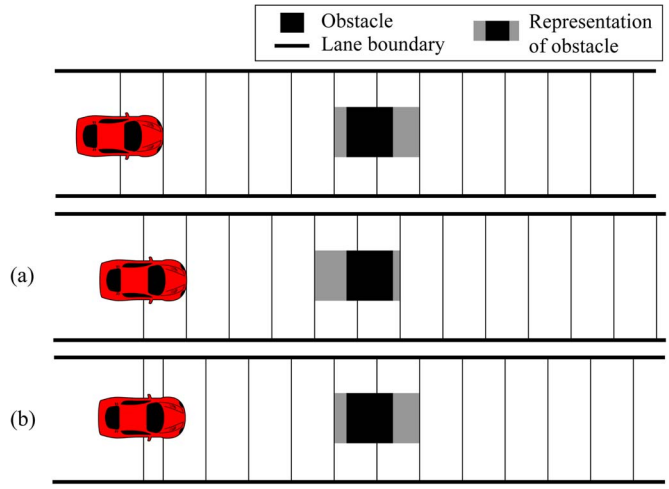

Fig. 5. Representation of the environment re-evaluated a short time later (a) without a correction time step and (b) with a correction time step.

Therefore, the sampling time, t_s, used in the zero-order hold discretization is given for the kth step into the horizon by:

$$t_s^{(k)} = \begin{cases} t_{s,\mathrm{MPC}} & 0 \le k < T_{\mathrm{split}} \\ t_{s,\mathrm{corr}} & k = T_{\mathrm{split}} \\ t_{s,\mathrm{long}} & T_{\mathrm{split}} < k \le (T-1) \end{cases} \tag{29}$$

where $t_{s,\mathrm{MPC}}$ is the controller execution time step, $t_{s,\mathrm{long}}$ is the longer time step used in the later portion of the horizon, and t_{corr} is the corrective, variable length time step.

The near-term time steps are shorter than the correction time step which is shorter than the long-term time steps, therefore any planned trajectory in the later portion of the horizon could also be planned in the near-term ensuring persistent feasibility of the optimal MPC solution.

D. Matching the Driver's Command

Cost term (25a) captures the desire to match the driver's steering command. This objective is best expressed using the l_1 norm for two reasons. First, the desire to *identically match* the driver's command is better captured by the larger values of the l_1 norm at small deviations than higher order norms as illustrated in Fig. 6. Second, in situations where significant deviation from the driver's command is required to ensure safety, it is desirable for the controller to ignore the driver as much as possible. The l_1 norm provides the best convex approximation to this objective because the value at large deviations is as small as possible while still being convex as discussed by Boyd and Vandenberghe [19].

E. Implementation

Optimization problem (25) is a convex quadratic program with a significantly sparse structure that can be exploited to produce an efficient solver for real-time implementation [20]. CVXGEN, developed by Mattingley and Boyd [21], generates a custom, primal-dual interior point solver that is implemented on a single core of an i7 processor utilizing MATLAB's real-time

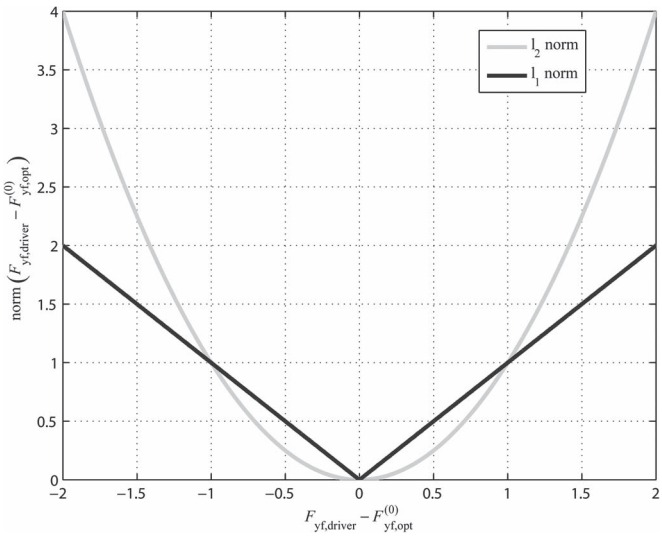

Fig. 6. Comparison of the l_1 and l_2 norms illustrating the different behavior of the norms at small values of $(F_{\mathrm{yf,driver}} - F^{(0)}_{\mathrm{yf,opt}})$ versus larger values.

TABLE II
CONTROLLER PARAMETERS

Parameter	Symbol	Value	Units
Surface friction coefficient	μ	0.55	(none)
Vehicle longitudinal speed	U_{x}	(measured)	$\frac{\mathrm{m}}{\mathrm{s}}$
Driver comfort distance	d_{buffer}	0.4	m
Prediction horizon length	T	30	(none)
Near-term horizon length	T_{split}	10	(none)
Controller time step size	$t_{s,\mathrm{MPC}}$	0.01	s
Correction time step size	$t_{s,\mathrm{corr}}$	(computed)	s
Later horizon time step size	$t_{s,\mathrm{long}}$	0.2	s
Near-term smooth input weight	γ_{near}	5	$\frac{1}{\mathrm{kN}^2}$
Long-term smooth input weight	γ_{long}	2	$\frac{1}{\mathrm{kN}^2}$
Stable handing slack weight	σ_{sh}	[60 60]	$\left[\frac{1}{\mathrm{rad}} \quad \frac{\mathrm{s}}{\mathrm{rad}}\right]$
Environmental slack weight	σ_{env}	1000	$\frac{1}{\mathrm{m}^2}$
Driver's commanded steer angle	δ_{driver}	(measured)	rad

toolbox. Table II gives the parameters used in the controller as implemented in the following experiments. These parameters give a look ahead time of 3.91 to 4.11 (s) depending on the present value of $t_{s,\mathrm{corr}}$. These parameters define an optimization problem for each tube that can be solved in less than 5 (ms). The number of optimization problems to be solved depends on the number of tubes needed to represent the environmental envelope.

In the worst-case, the number of tubes needed to represent the environmental envelope is 2^n, with n being the number of obstacles. This occurs in scenarios where each obstacle presents the controller with a choice of avoidance on the left or on the right. However, as the number of tubes grows, more of them can be ignored without affecting the performance of the controller because only the tube with the lowest optimal solution to optimization (25) determines the steering input applied to the vehicle. As illustrated in Fig. 7, many of the tubes in these worst-case environments unnecessarily weave between obstacles resulting in large optimal objective values to optimization (25) due to objective (25b). Therefore, heuristics could be employed to reduce the number of tubes to a representative handful that could be evaluated in real time. As mentioned

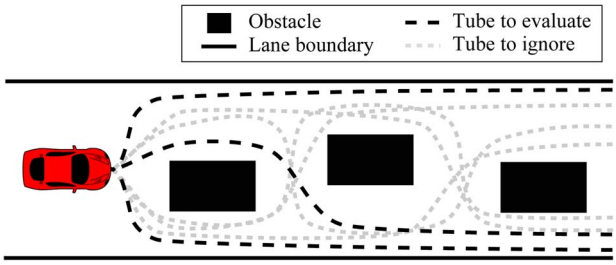

Fig. 7. An environment with 3 obstacles arranged in a manner that results in the worst-case number of possible tubes, $2^n = 8$. A single trajectory from each tube is illustrated. Many of the tubes unnecessarily weave around obstacles and can be ignored without affecting the optimal steering command.

Fig. 8. X1, an all electric steer-by-wire research testbed.

TABLE III
X1 VEHICLE PARAMETERS

Parameter	Symbol	Value	Units
Mass	m	1973	kg
Yaw moment of inertia	I_{zz}	2000	$\mathrm{kg \cdot m^2}$
Distance from front axle to CG	a	1.53	m
Distance from rear axle to CG	b	1.23	m
Width	d	1.87	m
Front cornering stiffness	$\mathrm{C}_{\alpha \mathrm{f}}$	100	kN/rad
Rear cornering stiffness	$\mathrm{C}_{\alpha \mathrm{r}}$	140	kN/rad

in Section IV-B, all tubes are considered at each execution of the controller without any regard to which tube produced the optimal steering command previously. Therefore, use of heuristics reduces the computational burden without restricting the driver to a single tube. The use of heuristics will be explored in future work.

V. EXPERIMENTAL VALIDATION

Experiments, using an instrumented test vehicle on a low friction surface, demonstrate the shared control scheme presented. In these experiments, the controller works with a human driver to negotiate obstacles along the reference line. The test vehicle is an all electric steer-by-wire vehicle called X1 which is shown in Fig. 8. The parameters for this vehicle are specified in Table III and were obtained using similar techniques as described by Laws *et al.* [22].

X1 is equipped with an integrated GPS/INS system that provides real-time estimates of the vehicle states. In these experiments, obstacles and road boundary locations are assumed to be known. All of the following experiments took place on a gravel surface with variable friction. Although real-time friction

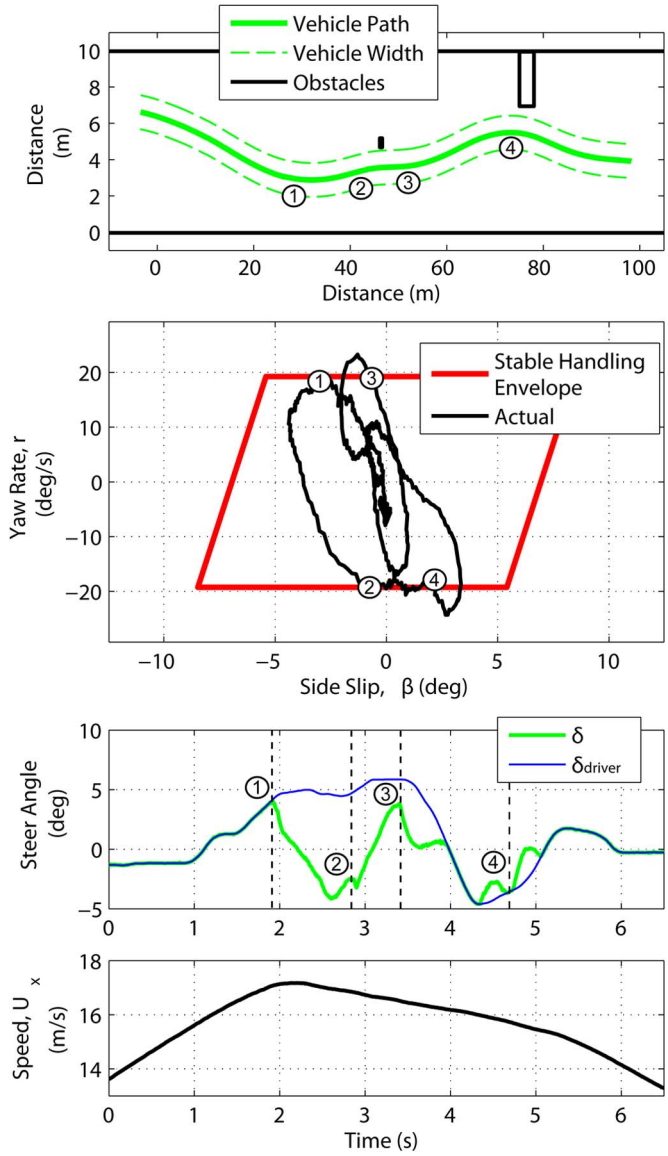

Fig. 9. Experiment on a low friction surface with a single obstacle in the middle of the road with a larger obstacle further down and on the left side of the road.

estimation has been demonstrated on vehicles equipped with steer-by-wire [1], a fixed estimate of friction is used for simplicity. During these experiments, the driver maintains full control of the vehicle's acceleration and braking, and the hand wheel in the vehicle's steer-by-wire system does not incorporate any artificial steering feel.

Fig. 9 illustrates a scenario in which the controller safely avoids a collision when the human driver takes no action to do so. In this scenario, a single obstacle lies in the middle of the road with a larger obstacle further down and on the left side of the road. As illustrated in the bottom of Fig. 9, the vehicle's speed, which is dictated by the driver, varies throughout the test. The simplifying assumption that the vehicle is maintaining a constant speed throughout the prediction horizon, which was addressed in Section III-B, does not negatively affect the controller's performance as the controller avoids collision with the environment while maintaining vehicle stability.

Initially, the controller identically matches the driver's command because doing so will not lead to a violation of either safe driving envelope. However, at instance ①, the driver's steering command threatens to violate the stable handling envelope, and the controller deviates from the driver's command to safely stabilize the vehicle. The controller continues to counter-steer the vehicle to avoid the approaching obstacle, and, at instance ②, the controller makes an additional steering adjustment to enforce both safe envelopes. The controller begins the process of again matching the driver's command. The rate of this transition is determined by γ_{near}. At instance ③, the controller makes a quick steering correction to maintain stability of the vehicle before identically matching the driver once again. This illustrates the importance of considering vehicle stability when transitioning between an automated system and a human driver. Despite the approaching parked car, the controller still identically matches the driver's command because his command safely avoids the obstacle. This illustrates the minimally invasive approach of envelope control. Two minor steering augmentations at instance ④ enforce the stable handling envelope.

Fig. 10 illustrates the controller's performance in a scenario where vehicle stability and obstacle avoidance directly compete. This is illustrated in a double lane change maneuver which conforms to ISO standard 3888-1 [23] on a low friction surface at speeds greater than 60 kph. At the start of the lane change, the controller identically matches the driver's steering command because doing so will not lead to a violation of either safe driving envelope. At instance ①, the driver prematurely initiates the first lane change and the controller makes a slight augmentation to prevent collision with the environment. The driver's command successfully completes the first lane change with only a slight correction made by the controller; however, at instance ②, the driver again prematurely initiates the lane change forcing the controller to modify his command. Once the obstacle has safely passed, the controller attempts to again match the driver's command at instance ③; however, the driver's command is too aggressive and threatens to violate both safe driving envelopes. The controller responds with a large augmentation of the driver's command to avoid colliding with the right road boundary.

At instance ④, the controller allows the vehicle to operate briefly outside the stable handling envelope to avoid collision with the road boundary. This illustrates the capability to evaluate the trade-off between vehicle stability and obstacle avoidance in real time. At instance ⑤, a large steering augmentation re-stabilizes the vehicle. Only 0.2 (s) separate instances ④ and ⑤, illustrating the importance of a fast controller execution rate in ensuring vehicle stability. The demanding maneuver presented in Fig. 10 also illustrates a limitation of the linear rear tire model used in the long-term prediction horizon. Without considering the future saturation of the rear tires, the controller attempts to match the driver at instance ③. If the driver's command had been ignored, violation of the safe envelopes may have been avoided. This can be addressed using the successive linearizations technique for handling nonlinearities in real-time MPC as explored by the authors [24]. However, despite the simplifying linear rear tire model in the long-term horizon, the controller successfully stabilizes the vehicle while safely navigating the environment in this demanding maneuver at high speed on low friction. In both experiments, $\Delta\psi = [-14 \quad 14]$ (deg) giving validation to the small angle approximations made in (15) and (16).

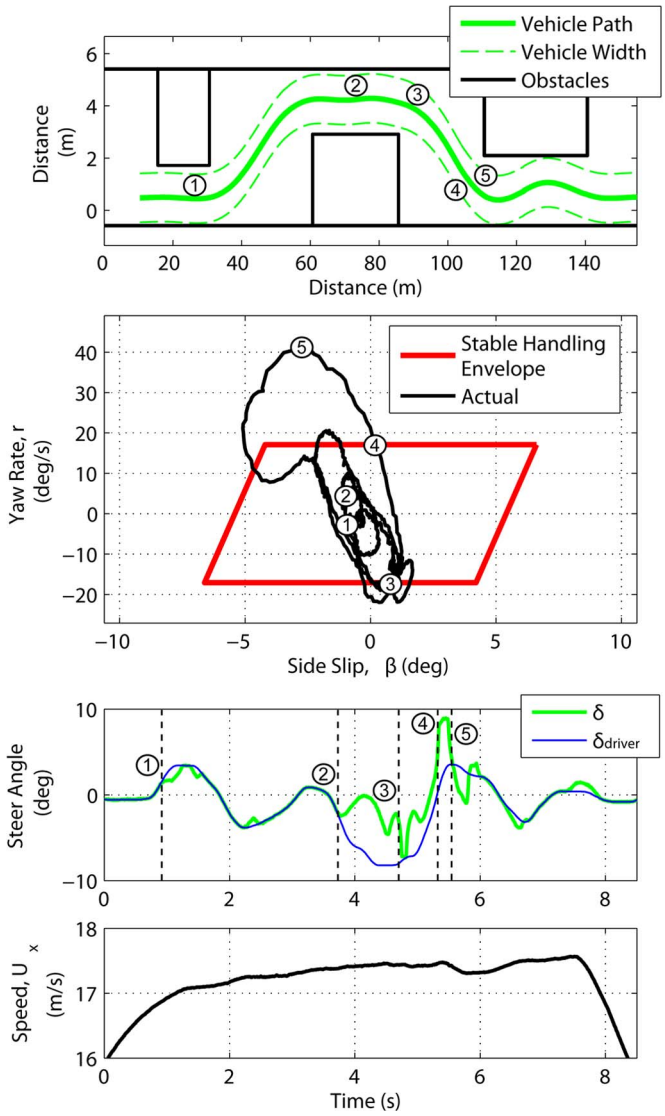

Fig. 10. Double lane change (ISO 3888-1) on a low friction surface.

VI. Conclusion

The constraint-based approach of envelope control enables vehicle safety while being minimally invasive to the driver. Experimental results demonstrate smooth integration of the controller's and driver's commands, showing promise of this approach as a shared control scheme without the need to model or interpret the driver's intentions. Dividing the environment into feasible tubes allows the use of fast convex optimization techniques resulting in a controller that can evaluate vehicle stability and obstacle avoidance at 100 (Hz) with a 4 (s) prediction horizon. In addition, dynamic maneuvers in an experimental testbed on a low friction surface illustrate the combined stabilizing and obstacle avoidance capabilities of the controller even in the presence of unmodeled disturbances.

ACKNOWLEDGMENT

The authors thank the Nissan Motor Company Ltd.; project team members Yoshitaka Deguchi and Hikaru Nishira for sponsoring this research; and John Kegelman, Daniel Malmquist, and Michael Erlie for their assistance in conducting experiments. The authors also gratefully acknowledge Jacob Mattingley and Stephen Boyd of the Information Systems Laboratory at Stanford University for providing real-time embedded optimization algorithms.

REFERENCES

[1] Y.-H. Hsu, S. Laws, and J. Gerdes, "Estimation of tire slip angle and friction limits using steering torque," *IEEE Trans. Control Syst. Technol.*, vol. 18, no. 4, pp. 896–907, Jul. 2010.

[2] T. Kawabe, H. Nishira, and T. Ohtsuka, "An optimal path generator using a receding horizon control scheme for intelligent automobiles," in *Proc. IEEE Int. Conf. Control Appl.*, Sep. 2004, vol. 2, pp. 1597–1602.

[3] N. M. Enache, S. Mammar, M. Netto, and B. Lusetti, "Driver steering assistance for lane-departure avoidance based on hybrid automata and composite Lyapunov function," *IEEE Trans. Intell. Transp. Syst.*, vol. 11, no. 1, pp. 28–39, Mar. 2010.

[4] A. Gray *et al.*, "Predictive control for agile semi-autonomous ground vehicles using motion primitives," in *Proc. ACC*, Jun. 2012, pp. 4239–4244.

[5] Y. Gao, T. Lin, F. Borrelli, E. Tseng, and D. Hrovat, "Predictive control of autonomous ground vehicles with obstacle avoidance on slippery roads," in *Proc. ASME Dyn. Syst. Control Conf.*, Sep. 2010, vol. 1, pp. 265–272.

[6] L. Saleh, P. Chevrel, F. Claveau, J.-F. Lafay, and F. Mars, "Shared steering control between a driver and an automation: Stability in the presence of driver behavior uncertainty," *IEEE Trans. Intell. Transp. Syst.*, vol. 14, no. 2, pp. 974–983, Jun. 2013.

[7] S. Anderson, S. Karumanchi, and K. Iagnemma, "Constraint-based planning and control for safe, semi-autonomous operation of vehicles," in *Proc. IEEE Intell. Veh. Symp.*, Jun. 2012, pp. 383–388.

[8] K. H. Well, "Aircraft control laws for envelope protection," in *Proc. AIAA Guid., Navigat., Control Conf.*, 2006, pp. 1–10.

[9] C. E. Beal and J. C. Gerdes, "Model predictive control for vehicle stabilization at the limits of handling," *IEEE Trans. Control Syst. Technol.*, vol. 21, no. 4, pp. 1258–1269, Jul. 2013.

[10] R. Attia, J. Daniel, J.-P. Lauffenburger, R. Orjuela, and M. Basset, "Reference generation and control strategy for automated vehicle guidance," in *Proc. IEEE IV*, Jun. 2012, pp. 389–394.

[11] F. Hundelshausen, M. Himmelsbach, F. Hecker, A. Mueller, and H.-J. Wunsche, "Driving with tentacles—Integrated structures of sensing and motion," *Int. J. Field Robot. Res.*, vol. 25, no. 9, pp. 640–673, 2008.

[12] C. R. Carlson and J. C. Gerdes, "Optimal rollover prevention with steer by wire and differential braking," in *Proc. ASME Int. Mech. Eng. Congr. Expo.*, Nov. 2003, vol. 1, pp. 345–354.

[13] S. M. Erlien, S. Fujita, and J. C. Gerdes, "Safe driving envelopes for shared control of ground vehicles," in *Proc. IFAC Symp. Adv. Automotive Control*, Sep. 2013, vol. 7, pp. 831–836.

[14] E. Fiala, "Lateral forces on rolling pneumatic tires," in *Zeitschrit V.D.I*, vol. 96, no. 29, p. 114, 1954.

[15] H. B. Pacejka, *Tire and Vehicle Dynamics*, 3rd ed. Oxford, U.K.: Butterworth-Heinemann, 2012.

[16] C. G. Bobier and J. C. Gerdes, "Staying within the nullcline boundary for vehicle envelope control using a sliding surface," *Veh. Syst. Dyn.*, vol. 51, no. 2, pp. 199–217, 2013.

[17] S. M. LaValle, *Planning Algorithms*. Cambridge, U.K.: Cambridge Univ. Press, 2006.

[18] S.-H. Suh and A. B. Bishop, "Collision-avoidance trajectory planning using tube concept: Analysis and simulation," *J. Robot. Syst.*, vol. 5, no. 6, pp. 497–525, Dec. 1988.

[19] S. Boyd and L. Vandenberghe, *Convex Optimization*. Cambridge, U.K.: Cambridge Univ. Press, 2004.

[20] J. Mattingley, Y. Wang, and S. Boyd, "Code generation for receding horizon control," in *Proc. IEEE Int. Symp. CACSD*, Sep. 2010, pp. 985–992.

[21] J. Mattingley and S. Boyd, "CVXGEN: A code generator for embedded convex optimization," *Optim. Eng.*, vol. 13, no. 1, pp. 1–27, 2012.

[22] S. M. Laws, C. D. Gadda, and J. C. Gerdes, "Frequency characteristics of vehicle handling: Model and experimental validation of yaw, sideslip, and roll modes to 8 Hz," in *Proc. AVEC 8th Int. Symp. Adv. Veh. Control*, Aug. 2011, Art. ID. 060211.

[23] *Passenger cars—Test track for a severe lane-change manoeuvre—Part 1: Double lane-change*, ISO Std. ISO 3888-1:1999(E), 1999.

[24] S. M. Erlien, J. Funke, and J. C. Gerdes, "Incorporating non-linear tire dynamics into a convex approach to shared steering control," in *Proc. Amer. Control Conf.*, Jun. 2014, pp. 3468–3473.

Stephen M. Erlien received the Ph.D. degree from Stanford University, Stanford, CA, USA, in 2015. He is currently the Controls Lead at Peloton-Technology, Mountain View, CA, where he applies shared control to heavy trucks to improve safety and efficiency. His research interests include human–computer shared control of dynamic systems and constraint-based control. Dr. Erlien was a recipient of a National Science Foundation Graduate Research Fellowship Award in 2009.

Susumu Fujita received the M.S. degree in system information sciences from Tohoku University, Sendai, Japan, in 2000. He is currently an Assistant Manager with Nissan Motor Company Ltd. His research interests include the design and development of collision avoidance and driver assistance systems with an emphasis on system architecture design. Mr. Fujita was a recipient of the Asahara Science Award from the 61th Society of Automobile Engineers of Japan in 2011.

Joseph Christian Gerdes received the Ph.D. degree from the University of California, Berkeley, CA, USA, in 1996. He is a Professor of mechanical engineering at Stanford University, Stanford, CA, and the Director of the Center for Automotive Research at Stanford (CARS). His laboratory studies how cars move, how humans drive cars, and how to design future cars that work cooperatively with the driver or drive themselves. When not teaching on campus, he can often be found at the racetrack with students, instrumenting historic race cars or trying out their latest prototypes for the future. Prof. Gerdes and his team have been recognized with several awards, including the Presidential Early Career Award for Scientists and Engineers, the Ralph Teetor Award from SAE International, and the Rudolf Kalman Award from the American Society of Mechanical Engineers.